

## Article

# Mechanical Properties of SMA/PVA-ECC under Uniaxial Tensile Loading

Zhao Yang <sup>1,2,\*</sup> , Jiankun Li <sup>1</sup>, Yilan Zhong <sup>1</sup> and Xiaolong Qi <sup>1</sup>

<sup>1</sup> School of Urban Construction, Wuhan University of Science and Technology, Wuhan 430065, China; dakun123@163.com (J.L.); hillwindcompany@163.com (Y.Z.); wy156182@163.com (X.Q.)

<sup>2</sup> Hubei Provincial Engineering Research Center of Urban Regeneration, Wuhan University of Science and Technology, Wuhan 430065, China

\* Correspondence: yzwh77@163.com

**Abstract:** Although shape memory alloy/Polyvinyl alcohol (SMA/PVA) hybrid fiber reinforced cementitious composites, (SMA/PVA-ECC) exhibit excellent crack closure and deformation recovery capabilities, however, the research on their fundamental mechanical properties is still limited. This study investigates the tensile mechanical properties of SMA/PVA-ECC materials by conducting uniaxial tensile tests, analyzing the failure behavior, stress–strain curves, and characteristic parameters of the specimens, comparing the influence of SMA fiber content and diameter, and establishing a tensile constitutive model. The results show that the residual crack width of SMA/PVA-ECC specimens significantly decreases after unloading, and SMA fiber content and diameter have a significant impact on the tensile properties of the specimens. The comprehensive tensile properties of specimens with a fiber diameter of 0.2 mm and content of 0.2% are the best, with their initial cracking strength, ultimate strength, and strain increasing by 56.4%, 23.6%, and 13.4%, respectively, compared to ECC specimens. The proposed bilinear tensile constitutive model has high accuracy. This study provides a theoretical basis for further research on SMA/PVA-ECC materials.

**Keywords:** SMA/PVA-ECC; superelasticity; tensile mechanical property; self-centering



**Citation:** Yang, Z.; Li, J.; Zhong, Y.; Qi, X. Mechanical Properties of SMA/PVA-ECC under Uniaxial Tensile Loading. *Buildings* **2023**, *13*, 2116. <https://doi.org/10.3390/buildings13082116>

Academic Editor: Xiaoyong Wang

Received: 28 June 2023

Revised: 9 August 2023

Accepted: 18 August 2023

Published: 21 August 2023



**Copyright:** © 2023 by the authors. Licensee MDPI, Basel, Switzerland. This article is an open access article distributed under the terms and conditions of the Creative Commons Attribution (CC BY) license (<https://creativecommons.org/licenses/by/4.0/>).

## 1. Introduction

Engineered Cementitious Composites (ECC) are a type of cement-based composite material that incorporates short fibers with specific types and performance characteristics into the cement matrix. ECC possesses various characteristics, such as multiple cracking and strain hardening, and its ultimate tensile strain is several hundred times greater than that of ordinary concrete [1]. ECC is widely used in civil engineering [2,3]. However, ECC typically employs a single fiber system, resulting in a relatively high-fiber fracture rate and a challenge in achieving both high strength and high ductility [4]. Additionally, ECC cannot provide crack closure and deformation self-recovery after unloading [5]. Its high ductility is still achieved at the cost of significant residual deformation damage.

By combining the superelastic Ni-Ti shape memory alloy (SMA) with the engineered cementitious composite (ECC), the hysteresis energy dissipation of SMA can increase the energy dissipation capacity of the composite material [6–9], and the shape recovery force of SMA after unloading can provide ECC with crack closure and deformation self-recovery [10], making it promising for self-recovering seismic structures. Compared with SMA wires or bars, SMA fibers do not require special connection anchorage. When SMA fibers are used in ECC, a new type of composite material Shape memory alloy and Polyvinyl alcohol fiber reinforced ECC (SMA/PVA-ECC) is formed. If the two materials are sufficiently bonded or anchored, the stress of the SMA fibers can increase with the load on the ECC matrix, causing a phase transition of the SMA material, exciting its superelasticity, resulting in larger strain and hysteresis energy dissipation characteristics, which can make ECC exhibit excellent energy dissipation ability. Meanwhile, after unloading,

SMA fibers can produce recovery force, which drives crack closure and ECC material deformation recovery. Additionally, randomly distributed SMA fibers can provide crack closure and deformation recovery for ECC in any direction [11]. The mechanical properties of ECC materials, created by mixing Ni-Ti-SMA and PVA fibers, were studied by ML Nehdi et al. [12,13]. The results showed that SMA fibers significantly improved the tensile and bending properties of ECC compared to ECC with only PVA fibers. Khakimova and Sherif [14,15] compared the effects of adding straight SMA fibers and hooked steel fibers at the end of mortar beams. The results showed that beams with straight SMA fibers had crack closure and self-recovery after unloading, compared with steel fibers. In our previous work, Yang et al. [16,17] conducted three-point bending cyclic loading tests and cyclic tensile tests on SMA/PVA-ECC specimens and found that SMA fibers with knotted ends could fully exert their superelastic properties, providing hysteresis energy dissipation capacity for the specimens and achieving crack closure and bending self-recovery functions, significantly improving the maximum tensile stress of the dog-bone specimens.

Currently, preliminary research on SMA/PVA-ECC has demonstrated its effectiveness in crack closure and deformation recovery. However, research on this new type of material is still in its infancy, and there is a lack of research results on its basic mechanical properties, especially on the tensile mechanical properties and theoretical models of the material. Therefore, this paper focuses on the tensile mechanical properties of SMA/PVA-ECC. Through uniaxial tensile tests, failure phenomena, stress, strain, and other mechanical performance indicators are studied, and the influence of SMA fiber content and diameter on tensile mechanical properties is compared. A constitutive model for tension is proposed.

## 2. Experimental Design

This part consists of three subsections. The first section is about material properties of ECC and SMA. The second section introduces the design scheme and manufacturing process of SMA/PVA-ECC test specimens. Then, the loading scheme of tensile test is introduced in the third section.

### 2.1. Material Properties

#### 2.1.1. Engineered Cementitious Composites (ECC)

Based on the references [18,19], the mix proportions were adjusted by considering the workability and flowability of the concrete mixture through experiments. Table 1 shows the final mix proportions with a sand–cement ratio of 0.2 and a water–cement ratio of 0.2. The raw materials for ECC included 52.5-grade Portland cement; Fly ash with a density of  $2.55 \text{ g/cm}^3$ , a fineness of  $16 \text{ }\mu\text{m}$ , and a moisture content of 0.85%; white crystal quartz sand with a main component of silicon dioxide and a particle size of 100 mesh; a high-efficiency polycarboxylate water-reducing agent with a dosage of 0.79% of the cement amount; and PVA fibers, produced by the KURARAY company in Japan, with a dosage of 2%, a density of  $1.3 \text{ g}\cdot\text{cm}^{-3}$ , a diameter of  $40 \text{ }\mu\text{m}$ —it has a length of 12 mm, a tensile strength of 1600 MPa, a modulus of elasticity of 39 GPa, and an elongation at a break of 7%.

**Table 1.** Mass proportion of engineered cementitious composites.

Raw Material	Cement	Fly Ash	Silica Sand	Water	Water Reducer	PVA/%
Mix proportion	1.0	4.0	0.20	0.22	0.0079	2% *

\* Percentage of fiber content by volume.

The uniaxial tensile test was conducted according to the Chinese standard JC/T 2461-2018 [20]. The stress–strain curve of the ECC material obtained from the uniaxial tensile test is shown in Figure 1. As shown from the graph, the ECC that was prepared with the test mix design has obvious strain hardening characteristics, with an ultimate strain exceeding 5%, and a tensile strength exceeding 4 MPa.

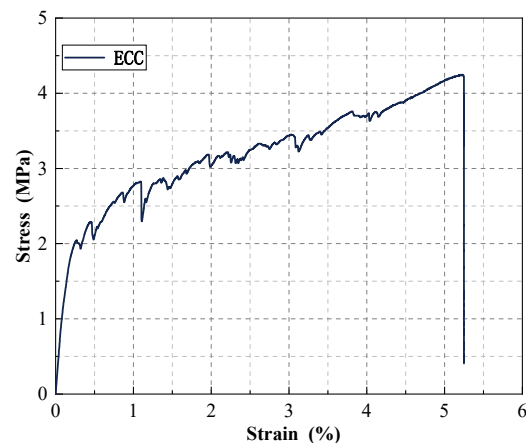


**Figure 1.** Uniaxial tensile stress–strain curve of ECC.

### 2.1.2. Shape Memory Alloys

The raw material used in the experiment to produce SMA fibers is SMA wire, which was produced by Jiangyin Renchang Nickel Titanium New Material Co., Ltd. (Jiangyin, China) with a density of  $6.49 \text{ g}\cdot\text{cm}^{-3}$ . The chemical composition of the SMA wire is primarily composed of 55.86% Ni and 44.14% Ti. The phase transition temperature of the wire was determined by differential scanning calorimetry (DSC). The austenite start and finish temperatures of the SMA wire were  $-34.60 \text{ }^\circ\text{C}$  and  $-18.19 \text{ }^\circ\text{C}$ , respectively, indicating that the SMA wire is in the austenite state at room temperature and can exhibit superelasticity. According to Reference [21], uniaxial tensile tests were conducted on SMA wires with diameters of 0.2 mm, 0.5 mm, and 1.0 mm to investigate the tensile mechanical properties of superelastic SMA. The effective tensile length (gage length) of the SMA wires was  $100 \pm 1 \text{ mm}$ , and the loading rate was  $2 \text{ mm}/\text{min}$ . The stress–strain curves at room temperature for the three diameters of SMA wire showed that they all exhibited a stress-induced martensitic phase transition at an applied strain of about 2%, resulting in an obvious strain plateau (Figure 2).

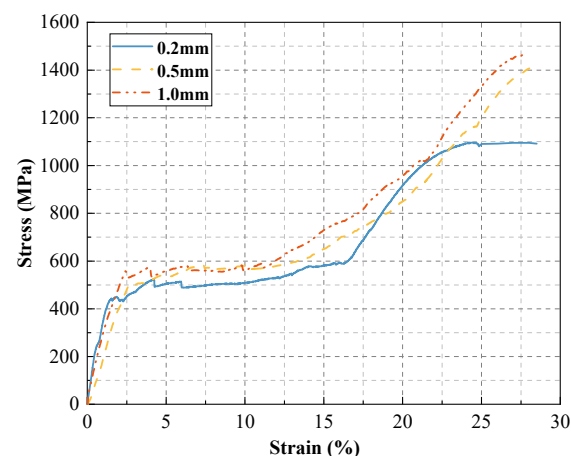


**Figure 2.** Uniaxial tensile stress–strain curve of the shape memory alloy.

## 2.2. SMA/PVA-ECC Specimen Design and Production

### 2.2.1. Specimen Design

The tensile mechanical properties and influencing factors of SMA/PVA-ECC composite materials were studied using uniaxial tensile tests. Dog-bone-shaped specimens were designed for the tensile tests, and their dimensions are shown in Figure 3. ECC materials were prepared using the mixing ratio in Table 1. To analyze the effects of SMA fiber diameter and content on the tensile properties of SMA/PVA-ECC composite materials,

three types of SMA fibers with diameters of 0.2 mm, 0.5 mm and 1.0 mm were selected, as well as three types of SMA fiber contents, which were 0.2%, 0.3% and 0.4%, SMA fiber content was controlled by weighing with an error kept within  $\pm 0.1$  g. Tensile specimens were designed and fabricated in nine groups of three specimens each, as shown in Table 2. SMA fibers were designed with knotted ends, and the length between the knotted ends was controlled at 40 mm. Figure 4 shows the design of the SMA fiber ends.

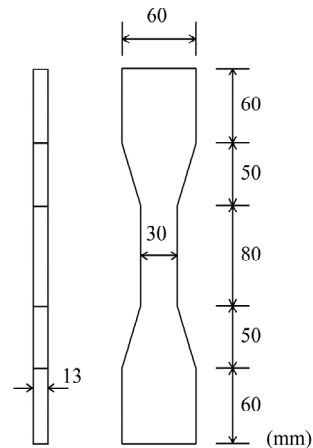


Figure 3. Specimen size.

Table 2. Specimen table of direct tension.

Specimen Number	SMA Diameter/mm	SMA Volume Content/%	PVA Volume Content/%	Number of Specimens
ECC	-	-	2	3
S-0.2-0.2	0.2	0.2	2	3
S-0.2-0.3		0.3	2	3
S-0.2-0.4		0.4	2	3
S-0.5-0.2	0.5	0.2	2	3
S-0.5-0.3		0.3	2	3
S-0.5-0.4		0.4	2	3
S-1.0-0.2	1.0	0.2	2	3
S-1.0-0.3		0.3	2	3
S-1.0-0.4		0.4	2	3

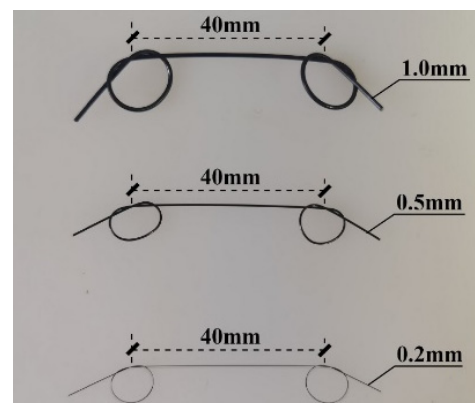
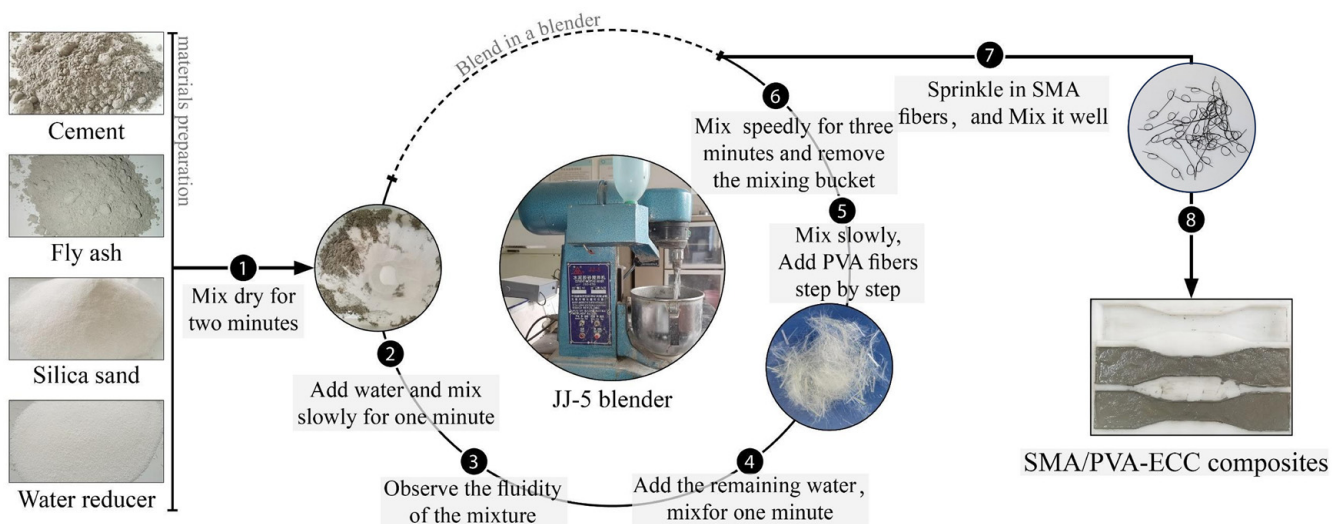


Figure 4. SMA fibers end shape.

### 2.2.2. Specimen Production

The powder materials (cement, fly ash, quartz sand, and the water-reducing agent) were poured into a JJ-5 type cement mortar mixer and dry mixed for two minutes until they were evenly dispersed. Approximately half of the required amount of water was added, and the mixture was stirred at a low speed for one minute. When the ingredients were completely mixed, the remaining water was added and stirred for another minute. PVA fibers were then added to the mixture, before removing the mixing bucket; the mixture was stirred at high speed for three minutes. Subsequently, batches of SMA fibers were sprinkled into the mixture and evenly stirred. Finally, the mixture was poured into the specimen molds to obtain the SMA/PVA-ECC composite material mixture. In the fabrication process, the main point was to ensure that the SMA fibers were uniformly distributed in the axial tensile direction of the specimen. After 24 h, the molds were removed, and the specimens were placed in a standard curing box with a temperature of  $20 \pm 2$  °C and a relative humidity of over 95% for 28 days. Figure 5 shows the detailed production process of the dog-bone-shaped tensile specimens.



**Figure 5.** Production process of the specimens.

### 2.3. Test Loading Scheme

As shown in Figure 6a, the uniaxial tensile test was conducted using a WD-PD6305 universal testing machine. In order to avoid stress concentration caused by direct contact between the specimen and the fixture, and to prevent eccentric tensile loading, the authors designed and fabricated a special tensile fixture to fix the dog-bone shaped specimen. The tensile fixture consists of upper and lower clamping ends, and upper and lower fixtures. To ensure a stable connection between the upper and lower clamping ends and the testing machine, the surface of the upper and lower clamping ends was subjected to 45° inclined scratching and polishing treatment. The schematic diagram of the tensile fixture is shown in Figure 6b. The test was conducted using displacement-controlled loading at a loading rate of 0.5 mm/min, and both the load and displacement were automatically recorded by the testing machine. The stress and strain were calculated based on the actual dimensions of the specimen. The loading was stopped when a clear main crack appeared on the specimen, and strain softening occurred.

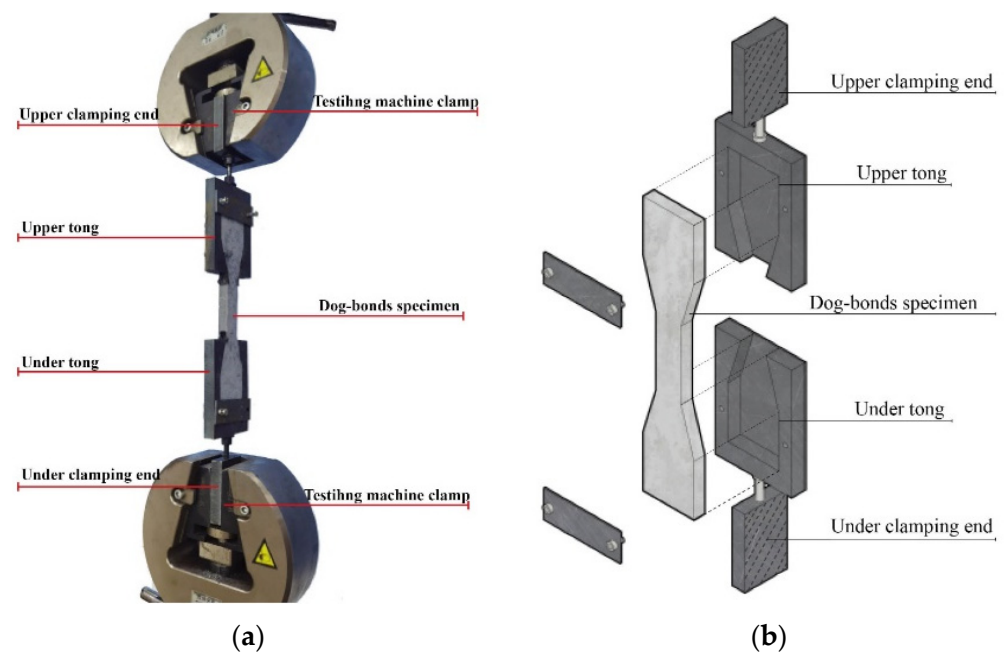


**Figure 6.** Test device design. (a) Testing device. (b) Diagram of tensile jig.

### 3. Results and Discussion

This part consists of five subsections. The first subsection analyzes and discusses the specimen failure behavior. The second subsection analyzes the stress–strain curves and compares the effects of SMA content and diameter. The third subsection presents the analysis of the experimental characterization parameters. The fourth subsection presents the analysis of SMA fiber strain. Finally, the tensile constitutive model is analyzed.

#### 3.1. Failure Behavior

Figure 7a presents the failure modes of ECC and SMA/PVA-ECC specimens during the loading and unloading process. All specimens exhibited distinct multiple cracking phenomena during the loading phase. From the crack development during loading, it can be observed that, initially, no cracks appeared on the surface of the specimen matrix, and the stress–strain curve exhibited almost linear growth. As loading continued, microcracks [22] gradually propagated from both ends of the specimen towards the center until saturation, with the width of the microcracks remaining relatively constant and did not exceed  $30\mu\text{m}$ . Ultimately, significant main cracks appeared in the middle of the specimen, leading to failure. During the failure phase, ECC specimens exhibited wider main cracks, which were unable to close effectively upon unloading. In contrast, SMA/PVA-ECC specimens demonstrated effective closure of both the main cracks and adjacent microcracks upon unloading. As an example, the comparison of cracks in SMA/PVA-ECC specimens during loading and after unloading was demonstrated using specimen S-0.5-0.2, as shown in Figure 7b. Taking specimens with a fiber content of 0.2% as an example for comparison (Table 3), it can be observed that specimens with different SMA fiber diameters had an average main crack width ranging from 2.44 mm to 3.14 mm during the failure phase, while the average residual crack width after unloading was only 0.34 mm to 0.47 mm, indicating a significant crack self-closing capability of SMA/PVA-ECC specimens. This is attributed to the sufficient anchoring performance of SMA fibers with knotted ends and ECC, as well as the effective utilization of the superelasticity of SMA fibers. Upon unloading, the SMA fibers generate recovery forces, effectively closing the cracks in the ECC matrix.



**Figure 7.** Failure mode of specimens. (a) ECC and SMA/PVA-ECC specimens. (b) Cracks comparison of S-0.5-0.2.

**Table 3.** Average value of crack width.

Specimen Number	Main Crack Width/mm	Residual Crack Width/mm
S-0.2-0.2	2.44	0.34
S-0.5-0.2	2.72	0.43
S-1.0-0.2	3.14	0.47

### 3.2. Stress–Strain Curve

#### 3.2.1. Comparative Analysis of ECC and SMA/PVA-ECC Specimens

In comparing the stress–strain curves of representative specimens in each group, it can be observed from Figure 8 that both ECC and SMA/PVA-ECC exhibit a three-stage development process with significant strain hardening characteristics. The curves showed multiple small fluctuations, indicating the presence of significant multiple cracking characteristics in the specimens. The comparison reveals that, compared to ECC specimens containing only PVA fibers, SMA/PVA-ECC specimens containing hybrid fibers exhibit a significant increase in initial cracking strength, and some hybrid fiber specimens show improved ultimate tensile stress. After reaching peak stress, the stress degradation of SMA/PVA-ECC is slower than that of ECC specimens, indicating that even after the PVA fibers are completely pulled or extracted, the SMA fibers can still bear loads under the anchoring effect of the knotted end, slowing down the rate of stress degradation. However, the ultimate strain of the SMA/PVA-ECC specimens is relatively lower than that of ECC specimens, with only a few hybrid fiber specimens exhibiting higher strain capacity than the ECC specimens.

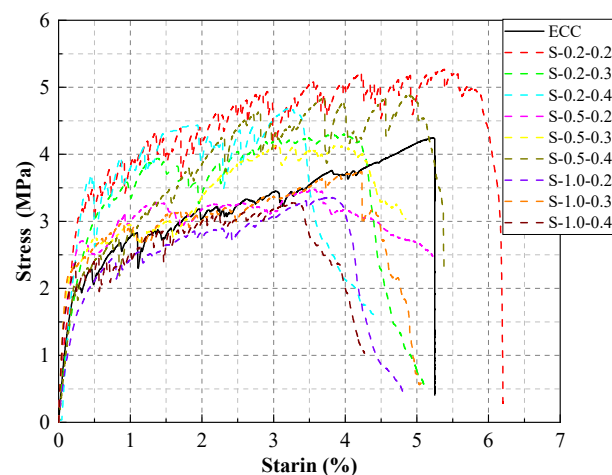


**Figure 8.** Tensile stress–strain curve of ECC, SMA/PVA-ECC.

### 3.2.2. Factors Affecting SMA/PVA-ECC Specimens

- SMA fiber content

Figure 9 shows the stress–strain curves of SMA/PVA-ECC specimens with different amounts of SMA fibers of the same diameter. From Figure 9a, it can be observed that, compared to ECC specimens, SMA/PVA-ECC specimens with 0.2 mm diameter fibers generally increase the ultimate tensile strength of the composite material. When the fiber content is 0.2%, the specimen exhibits the highest ultimate tensile stress and strain. The specimens with 0.3% and 0.4% fiber content have similar ultimate tensile stress and strain, but both are lower than that of the 0.2% fiber content specimen. This is because with a higher fiber content, there are more SMA fibers prone to aggregating during the pouring process, partially hindering the flow of the matrix, and resulting in internal pores and trapped air in the specimens, thus increasing internal defects. From Figure 9b, the ultimate tensile stress and strain of the SMA/PVA-ECC specimens with 0.5 mm diameter fibers increases with increasing fiber content. Among them, the specimen with 0.4% fiber content (S-0.5-0.4) has a higher ultimate tensile stress than ECC, but the ultimate strain is still lower than ECC. The ultimate tensile stress and strain of the other two groups of specimens with different fiber content are lower than those of ECC specimens. From Figure 9c, it is shown that, for SMA/PVA-ECC specimens with 1.0 mm diameter fibers, the specimen with 0.3% fiber content has the highest ultimate stress and strain, but it is still lower than that of ECC specimens. Therefore, as the content of small-diameter fibers decreases, the tensile performance of the specimens improves. On the other hand, for large-diameter fibers, the optimal tensile performance is achieved at a moderate fiber content.

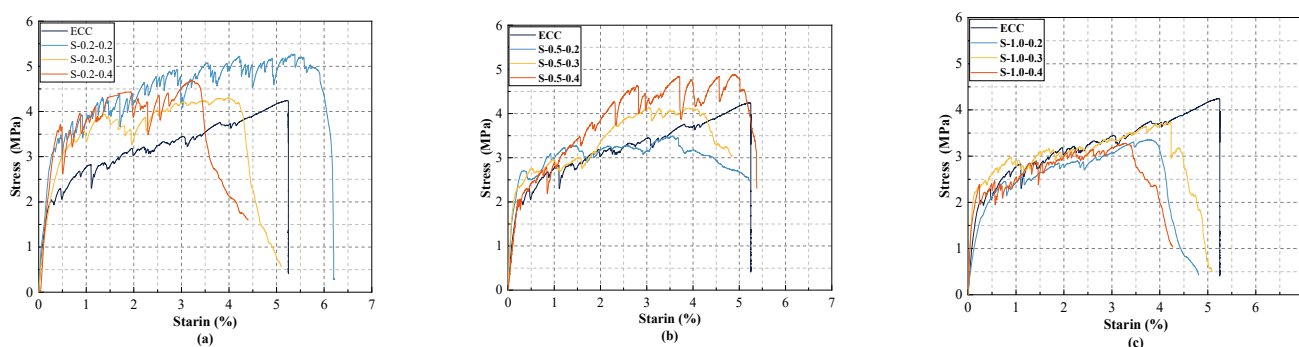


**Figure 9.** Stress–strain curves of SMA/PVA-ECC with different content of SMA fibers of the same diameter. (a) Specimens with SMA fiber diameter 0.2 mm. (b) Specimens with SMA fiber diameter 0.5 mm. (c) Specimens with SMA fiber diameter 1.0 mm.

- SMA fiber diameter

SMA/PVA-ECC specimens with different diameters of SMA fibers but with the same content are shown in Figure 10. As shown in Figure 10a,b, when the content is the same, specimens with smaller diameter SMA fibers exhibit higher ultimate tensile strength and strain than those with larger diameter SMA fibers. This is because the tensile strength of the composite material is mainly determined by the fiber bridging stress, and at the same fiber content, a higher number of small-diameter SMA fibers compared to large-diameter SMA fibers results in an increased bridging force provided by the SMA fibers, thereby enhancing the strength and deformation capacity of the SMA/PVA-ECC composite material. However, as analyzed from Figure 10c, beyond a certain content, the finer diameter SMA fibers may cause negative hybridization effects due to clustering, resulting in the tensile strength of the composite material specimens (S-0.2-0.4) being similar to that of specimens with coarser diameter SMA fibers (S-0.5-0.4). Therefore, when the content is lower, specimens with smaller diameter SMA fibers exhibit better tensile properties, while specimens with intermediate diameter fibers exhibit the best tensile properties at a certain higher content.

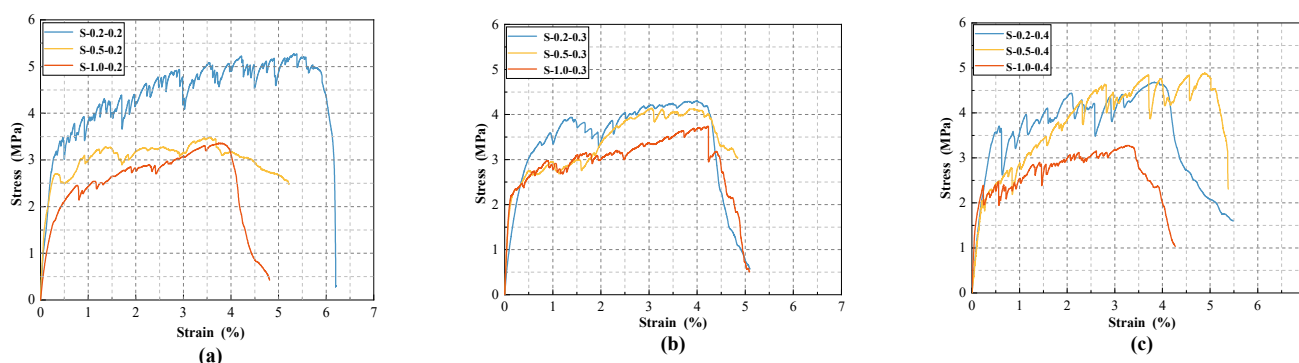


**Figure 10.** Stress–strain curves of SMA/PVA-ECC with different diameter of SMA fibers of the same content. (a) Specimens with SMA fiber content 0.2%. (b) Specimens with SMA fiber content 0.3%. (c) Specimens with SMA fiber content 0.4%.

### 3.3. Analysis of Test Characteristic Parameters

The characteristic parameters of the stress–strain curves of the specimens, under the uniaxial tensile test, are shown in Table 4. All the data in the table represent the average values of three specimens with the same identification number. The standard deviation of ECC specimens ranges from 2% to 3%, while the standard deviations of specimens with 0.2 mm, 0.5 mm, and 1.0 mm diameter SMA fibers are between 4% to 6%, 5% to 7%, and 3% to 7%, respectively. According to Table 4, the ECC containing only PVA fibers has a relatively low initial cracking strength of 2.04 MPa. The determination of the initiation of cracks is based on the stress–strain curve, wherein the occurrence of the first discernible fluctuation in the curve indicates the presence of the initial crack in the specimen. The addition of SMA fibers enhances the initial cracking strength of the SMA/PVA-ECC specimens, which ranges from 2.05 MPa to 3.57 MPa. Among them, the initial cracking strength and ultimate strength of the SMA/PVA-ECC with a fiber diameter of 0.2 mm were improved. The initial cracking strengths of the three types of mixed fiber composite materials with different fiber contents were improved by 56.4%, 54.4%, and 75%, respectively, compared to ECC. The ultimate strengths were increased by 23.6%, 1.4%, and 10.4%, respectively. The addition of SMA fibers resulted in a decrease in the deformation ability of most SMA/PVA-ECC specimens. Only the SMA/PVA-ECC specimen (S-0.2-0.2), with a fiber diameter of 0.2 mm and a content of 0.2%, showed an increase of 13.4% in ultimate tensile strain compared to ECC. Therefore, the SMA/PVA-ECC exhibits the best tensile performance when the SMA fiber has a diameter of 0.2 mm and a content of 0.2%.

**Table 4.** Characteristic parameters of the tensile stress–strain curve.

Number	Cracking Strength/MPa	Cracking Strain/%	Tensile Strength/MPa	Tensile Strain/%
ECC	2.04	0.26	4.24	5.23
S-0.2-0.2	3.19	0.33	5.24	5.93
S-0.2-0.3	3.15	0.56	4.30	4.01
S-0.2-0.4	3.57	0.48	4.68	3.83
S-0.5-0.2	2.71	0.32	3.43	3.56
S-0.5-0.3	2.35	0.23	4.09	4.10
S-0.5-0.4	2.05	0.21	4.88	4.89
S-1.0-0.2	2.07	0.47	3.36	3.83
S-1.0-0.3	2.23	0.14	3.81	4.32
S-1.0-0.4	2.39	0.23	3.31	3.91

### 3.4. SMA Fiber Strain Analysis

In the ECC matrix, the knotted end can provide sufficient anchoring force for the SMA fibers. It can be assumed that there is no relative slip between the knotted end and the ECC

matrix. For any single SMA fiber, its length after tensile deformation  $L'_f$  can be taken as the sum of its initial length  $L_f$  and the crack width  $W$  of the matrix, as shown in Figure 11.

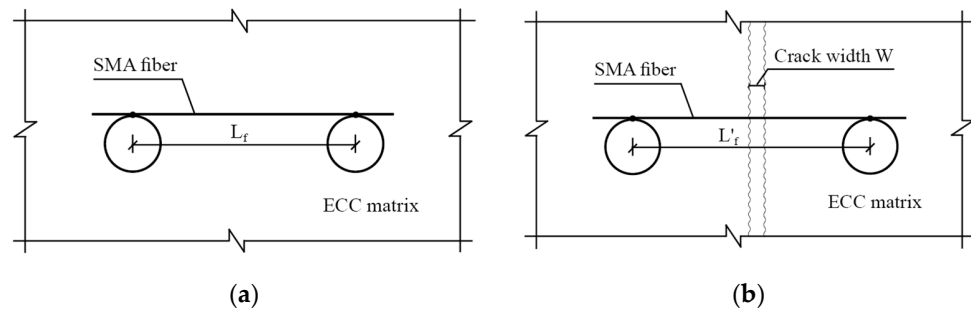


**Figure 11.** Schematic diagram of SMA fiber deformation. (a) Before cracking. (b) After cracking.

Therefore, the strain of the SMA fiber can be expressed using the following formula:

$$\varepsilon_f = \frac{W}{L_f} \quad (1)$$

According to Equation (1), the SMA fiber strains at the main crack locations of each specimen can be calculated. Taking the three groups of specimens listed in Table 4 as examples, calculations were performed, and the results are presented in Table 5. It is shown in Table 5 that the SMA fiber strains at the main crack locations of all specimens were between 6.1% and 7.9%, which exceeded the critical transformation strain of 2%. Combined with the SMA direct tensile stress–strain curve (Figure 2), it can be concluded that the stress in the SMA fibers at the main crack locations can reach 550 MPa to 600 MPa. This indicates that the knotted SMA fibers at the main crack locations can reach the martensite transformation state induced by stress and that the SMA fibers can effectively exhibit superelasticity.

**Table 5.** The strain of the SMA fiber at the main crack.

Specimen Number	Main Crack Width/mm	Strain of SMA Fiber/%
S-0.2-0.2 (0.3, 0.4)	2.44	6.1%
S-0.5-0.2 (0.3, 0.4)	2.72	6.8%
S-1.0-0.2 (0.3, 0.4)	3.14	7.9%

NOTE: All average value in this table.

### 3.5. Tensile Constitutive Model

Based on the stress–strain curves obtained from the SMA-ECC specimens in this test, and referring to the bilinear relationship theory proposed by Tetsushi Kanda et al. for randomly short fiber reinforced cement composites [23], a bilinear hardening model is proposed to describe the constitutive behavior of SMA-ECC material under tension, as shown in Figure 12.

To minimize the influence of initial eccentricity and initial torque on the curve, the concept of fitting crack initiation point  $(\sigma_c, \varepsilon_c)$  is introduced, which is defined as the intersection point of the fitting line OA in the elastic stage and the fitting line AB in the strain hardening stage. The simplified axial constitutive relationship is expressed as Equations (2) and (3) [22].

$$\sigma(\varepsilon) = \begin{cases} E_c \varepsilon & 0 \leq \varepsilon \leq \varepsilon_c \\ \sigma_c + E_t(\varepsilon - \varepsilon_c) & \varepsilon_c < \varepsilon \leq \varepsilon_t \end{cases} \quad (2)$$

$$E_t = \frac{\sigma_t}{\varepsilon_t} \quad (3)$$

where,  $\varepsilon_t$  is the ultimate strain, and  $\sigma_t$  is the ultimate strength.

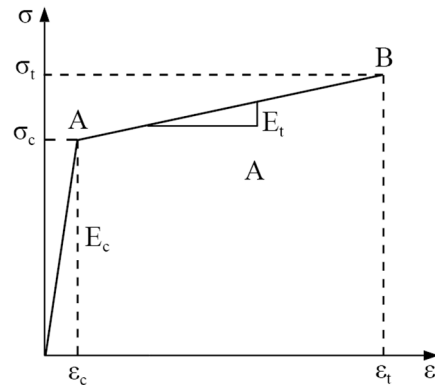


**Figure 12.** Simplified model of SMA-ECC stress–strain curve.

Three groups of test curves from specimens, with a 0.2 mm SMA fiber diameter but different contents, were selected for comparison. The characteristic point parameters were calculated from the experimental data, and the comparison results are shown in Figure 13. It is shown that the bilinear model fits well with the experimental curves, indicating that the bilinear constitutive model proposed in this paper is accurate.

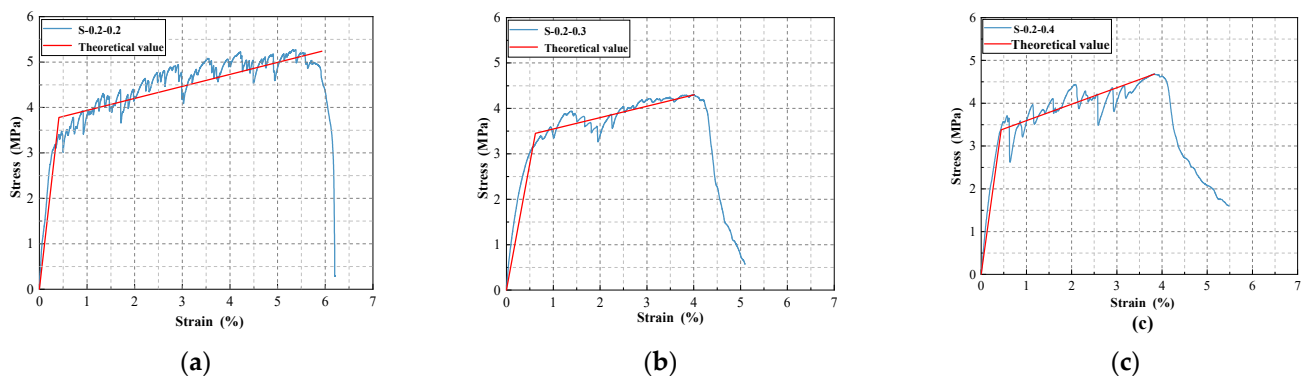


**Figure 13.** Comparison of theoretical and experimental values. (a) S-0.2-0.2. (b) S-0.2-0.3. (c) S-0.2-0.4.

#### 4. Conclusions

This paper presents a study on the tensile mechanical properties and theoretical models of SMA-PVA hybrid fiber-reinforced cementitious composites. The research reveals that the residual crack width of SMA/PVA-ECC specimens significantly decreases after unloading, and the material strength notably increases. The content and diameter of SMA fibers have a substantial impact on the tensile performance of the specimens. The proposed bilinear tensile constitutive model can provide a relatively accurate representation of the tensile behavior of this composite material. The main conclusions are as follows:

- (1) The knotted SMA fibers exhibit good anchoring performance with ECC, as well as good superelastic characteristics. After unloading, the micro-cracks in the SMA/PVA-ECC specimens are effectively closed, and the residual width of the main crack is significantly reduced.
- (2) The stress–strain curve of SMA/PVA-ECC exhibits a three-stage development process and obvious strain-hardening characteristics. The addition of SMA fibers improves the initial cracking strength and some ultimate strength of the composite specimens. After reaching the peak stress, the stress degradation of SMA/PVA-ECC is slower than that of ECC specimens, but most of the ultimate strains are lower than that of ECC.

- (3) The diameter and content of SMA fibers have a significant effect on the tensile properties of SMA/PVA-ECC. The smaller the diameter and content of the fiber, the better the tensile performance of the specimen. When the content of large-diameter fibers is moderate, the tensile performance of the specimen is the best. At low content, the tensile performance of small-diameter fiber specimens is better, and when exceeding a certain content, the tensile performance of medium-diameter fiber specimens is the best. Among them, the specimen with a fiber diameter of 0.2 mm and a content of 0.2% has the best comprehensive tensile performance, with an increase in initial cracking strength, ultimate strength, and strain of 56.4%, 23.6% and 13.4%, respectively, compared with ECC specimens.
- (4) The bilinear hardening model used in this study can well reflect the tensile stress–strain relationship of SMAF-ECC composite materials.

**Author Contributions:** Conceptualization, Z.Y.; methodology, Z.Y.; software, J.L.; formal analysis, J.L. and Y.Z.; investigation, J.L. and Y.Z.; data curation, J.L. and X.Q.; writing—original draft preparation, J.L. and Y.Z.; writing—review and editing, Z.Y.; visualization, J.L. and X.Q.; supervision, Z.Y.; project administration, Z.Y.; funding acquisition, Z.Y. All authors have read and agreed to the published version of the manuscript.

**Funding:** This research was funded by The National Natural Science Foundation of China, grant number 52178158; The Excellent Young and Middle-aged Science and Technology Innovation Team Plan of Hubei Provincial Department of Education, grant number Zy2022e004; The Science and Technology Plan Project of Department of Housing and Urban-Rural Development of Hubei Province, grant number (2022)2198-76.

**Data Availability Statement:** The processed data required to reproduce these findings cannot be shared at this time as the data also forms part of an ongoing study.

**Conflicts of Interest:** The authors declare no conflict of interest.

## References

1. Pakravan, H.R.; Jamshidi, M.; Latifi, M. The effect of hybridization and geometry of polypropylene fibers on engineered cementitious composites reinforced by polyvinyl alcohol fibers. *J. Compos. Mater.* **2016**, *50*, 1007–1020. [[CrossRef](#)]
2. Arce, G.A.; Noorvand, H.; Hassan, M.M.; Rupnow, T.; Dhakal, N. Feasibility of low fiber content PVA-ECC for jointless pavement application. *Constr. Build. Mater.* **2021**, *268*, 121131. [[CrossRef](#)]
3. Arce, G.; Noorvand, H.; Hassan, M.; Rupnow, T.; Hungria, R. Cost-effective ECC with low fiber content for pavement application. In *MATEC Web of Conferences*; EDP Sciences: Les Ulis, France, 2019; Volume 271, p. 07001.
4. Feng, Z.; Zhou, Y.; Sui, L.; Zhu, Z. Optimal design of a low-cost high-performance hybrid fiber engineered cementitious composites. *Constr. Build. Mater.* **2022**, *345*, 128372. [[CrossRef](#)]
5. Dehghani, A.; Aslani, F. Crack recovery and re-centring performance of cementitious composites with pseudoelastic shape memory alloy fibres. *Constr. Build. Mater.* **2021**, *298*, 123888. [[CrossRef](#)]
6. Andrawes, B.; DesRoches, R. Unseating prevention for multiple frame bridges using superelastic devices. *Smart Mater. Struct.* **2005**, *14*, S60. [[CrossRef](#)]
7. Fang, C.; Wang, W. *Shape Memory Alloys for Seismic Resilience*; Springer: Singapore, 2020.
8. Dizaji, F.S.; Dizaji, M.S. Seismic performance assessment of steel frames upgraded with shape memory alloy re-centering dampers for passive protection of structures subjected to seismic excitations using high-performance NiTiHfPd material. *Smart Mater. Struct.* **2022**, *31*, 065004. [[CrossRef](#)]
9. Zhou, X.; Ke, K.; Yam, M.C.; Zhao, Q.; Huang, Y.; Di, J. Shape memory alloy plates: Cyclic tension-release performance, seismic applications in beam-to-column connections and a structural seismic demand perspective. *Thin-Walled Struct.* **2021**, *167*, 108158. [[CrossRef](#)]
10. Li, X.; Li, M.; Song, G. Energy-dissipating and self-repairing SMA-ECC composite material system. *Smart Mater. Struct.* **2015**, *24*, 025024. [[CrossRef](#)]
11. Indhumathi, S.; Dinesh, A.; Pichumani, M. Diverse perspectives on self healing ability of Engineered Cement Composite–All-inclusive insight. *Constr. Build. Mater.* **2022**, *323*, 126473.
12. Ali, M.A.E.M.; Soliman, A.M.; Nehdi, M.L. Hybrid-fiber reinforced engineered cementitious composite under tensile and impact loading. *Mater. Des.* **2017**, *117*, 139–149. [[CrossRef](#)]
13. Ali, M.A.; Nehdi, M.L. Experimental investigation on mechanical properties of shape memory alloy fibre-reinforced ECC composite. In *Proceedings of the 11th International Conference on Civil and Architecture Engineering*, Military Technical College, Cairo, Egypt, 19–21 April 2016; Volume 11, pp. 1–11.

14. Khakimova, E.; Sherif, M.M.; Ozbulut, O.E.; Harris, D.K.; Ozyildirim, H.C. Experimental investigations on shape memory alloy fiber reinforced concrete. In Proceedings of the 6th International Conference on Advances in Experimental Structural Engineering, 11th International Workshop on Advanced Smart Materials and Smart Structures Technology, University of Illinois, Urbana-Champaign, Champaign, IL, USA, 1–2 August 2015.
15. Sherif, M.M.; Khakimova, E.M.; Tanks, J.; Ozbulut, O.E. Cyclic flexural behavior of hybrid SMA/steel fiber reinforced concrete analyzed by optical and acoustic techniques. *Compos. Struct.* **2018**, *201*, 248–260. [[CrossRef](#)]
16. Yang, Z.; Deng, T.; Li, J.; Xu, C. Experimental Study on Self-Centering Performance of the SMA Fiber Reinforced ECC Composite Beam. *Materials* **2022**, *15*, 3062. [[CrossRef](#)] [[PubMed](#)]
17. Yang, Z.; Du, Y.; Liang, Y.; Ke, X. Mechanical Behavior of Shape Memory Alloy Fibers Embedded in Engineered Cementitious Composite Matrix under Cyclic Pullout Loads. *Materials* **2022**, *15*, 4531. [[CrossRef](#)] [[PubMed](#)]
18. Ma, R.; Guo, L.; Ye, S.; Sun, W.; Liu, J. Influence of hybrid fiber reinforcement on mechanical properties and autogenous shrinkage of an ecological UHPFRCC. *J. Mater. Civ. Eng.* **2019**, *31*, 04019032. [[CrossRef](#)]
19. Meng, W.; Khayat, K.H. Effect of hybrid fibers on fresh properties, mechanical properties, and autogenous shrinkage of cost-effective UHPC. *J. Mater. Civ. Eng.* **2018**, *30*, 04018030. [[CrossRef](#)]
20. *JC/T2461-2018*; Standard Test Method for the Mechanical Properties of Ductile Fiber Reinforced Cementitious Composites. China Building Industry Press: Beijing, China, 2018.
21. Fathi, H.; Shokrieh, M.M.; Saeedi, A. Effect of tensile loading rate on interfacial properties of SMA/polymer composites. *Compos. Part B Eng.* **2020**, *183*, 107730. [[CrossRef](#)]
22. Liu, H.; Zhang, Q.; Gu, C.; Su, H.; Li, V. Influence of microcrack self-healing behavior on the permeability of Engineered Cementitious Composites. *Cem. Concr. Compos.* **2017**, *82*, 14–22. [[CrossRef](#)]
23. Kanda, T.; Lin, Z.; Li, V.C. Tensile stress-strain modeling of pseudostrain hardening cementitious composites. *J. Mater. Civ. Eng.* **2000**, *12*, 147–156. [[CrossRef](#)]

**Disclaimer/Publisher's Note:** The statements, opinions and data contained in all publications are solely those of the individual author(s) and contributor(s) and not of MDPI and/or the editor(s). MDPI and/or the editor(s) disclaim responsibility for any injury to people or property resulting from any ideas, methods, instructions or products referred to in the content.